Damage prediction in the vicinity of an impact on a concrete structure: a combined FEM/DEM approach.

Jessica ROUSSEAU, Emmanuel FRANGIN, Philippe MARIN, Laurent DAUDEVILLE

Université Joseph Fourier/INPG/CNRS

Laboratoire Sols, Solides, Structures, Risques (3S-R)

DU BP53, 38041 Grenoble Cedex 9 France

Corresponding Author: jessica.rousseau@hmg.inpg.fr

Abstract

This article focuses on concrete structures submitted to impact loading and is aimed at predicting local damage in the vicinity of an impact zone as well as the global response of the structure. The Discrete Element Method (DEM) seems particularly well suited in this context for modeling fractures. An identification process of DEM material parameters from macroscopic data (Young's modulus, compressive and tensile strength, fracture energy, etc.) will first be presented for the purpose of enhancing reproducibility and reliability of the simulation results with DE samples of various sizes.

The modeling of a large structure by means of DEM may lead to prohibitive computation times. A refined discretization becomes required in the vicinity of the impact, while the structure may be modeled using a coarse FE mesh further from the impact area, where the material behaves elastically. A coupled discrete-finite element approach is thus proposed: the impact zone is modeled by means of DE and elastic FE are used on the rest of the structure. The proposed approach is then applied to a rock impact on a concrete slab in order to validate the coupled method and compare computation times.

1. Introduction

The design of some civil engineering structures must take into account the risk of severe loadings due to natural or manmade hazards, such as rockfalls, aircraft or missile impacts. On a sensitive concrete structure, such loadings may have disastrous consequences, and an efficient and accurate prediction of damage proves to be of prime importance. Generally speaking, these severe loadings lead to fractures and fragmentation localized in one part of the concrete structure. The Discrete Element Method (DEM) (Cundall and Strack, 1979) is appropriate for modeling such discontinuities. The model developed uses a disordered assembly of spherical elements of different sizes and masses in order to reproduce isotropic and homogeneous behavior at the macroscopic scale. This method does not rely on any assumption regarding where and how a crack or several cracks occur and propagate since the medium is naturally discontinuous and very well adapted to dynamic problems. In order to offer a predictive model, the DE model must properly depict concrete behavior.

The identification process of Discrete Element (DE) parameters, in both linear and nonlinear behavior, will first be described. Local model parameters are calibrated so as to reproduce macroscopic concrete behavior. This process is nearly the same as that described in Hentz *et al.* (2004a), and the proposed modifications have simplified the process and improved the reproducibility and accuracy of the macroscopic characteristics obtained. These improvements have also provided a reliable and fast calibration method for parameters of large structures.

Nevertheless, computation time increases with the number of DE, and the analysis of large structures with DEM proves difficult. A number of authors have pointed out that such a method is limited to small structures due to the computation cost of DEM. Use of the FE method further from the impacted area represents one way to minimize this constraint since in

most cases, severe degradation phenomena are localized right in the vicinity of the impact. In addition, the FE method is widely used, and efficient mesh generation software can dramatically reduce modeling duration, with the potential for faster calculations than when applying a full DE approach thanks to the facility of handling various discretization sizes. These facts naturally lead to proposing a coupled FE/DE approach. Such a coupling is based on partitioning the structure into two sub-domains: an initial FE domain where nonlinear phenomena may be neglected, and a second DE domain where severe nonlinear degradation phenomena due to impact loading may occur. The second section of this article will summarize the main features of the coupling method. Additional technical details can be found in another paper by the same authors (Frangin *et al.*, 2006).

In the fourth section of this article, the coupling method will be used for modeling a rock impact on a concrete slab. This part is intended to illustrate, by way of example, the identification process, validation of the coupling method through a comparison between a DE model and a coupled FE/DE model, and the computation time-savings offered by the coupled model.

2. The Discrete Element model for concrete

2.1 Model description

Discrete methods can be split into two groups: lattice models and discrete element models. Lattice models use simple deformable elements like beams or bars organized into a structural network; these models are widely used to represent concrete at the microscopic or mesolevel scale (Leite *et al.*, 2004; Prado and Van Mier, 2003). For example, Prado and Van Mier (2003) modeled concrete material according to three phases: aggregates, mortar and interfaces. They used 2D Euler-Bernoulli beams with elastic and fully brittle constitutive behavior. Such models perform poorly when it comes to representing the contact between

fractured areas, and a fine discretization scale is required. The extension to 3D models therefore is hardly feasible.

More recently, Berton and Bolander (2005) developed a lattice model with Voronoi discretization. This model, based on the Rigid-Body-Spring Model (Kawai, 1978), has been used to simulate mode I fracture in concrete. For more general loading conditions, such as compression, the work of Shlangen and Garboczi (1997) and Cusatis and Cedolin (2007) merits recognition. Cusatis and Cedolin (2007) have developed a new lattice model called the "Confinement Shear Lattice model". They only considered the largest aggregates and connected the centroids with structural elements. An associated behavior for each element takes mortar, smaller aggregates and the cement-aggregate interface all into account. For this reason, modeled systems may actually be larger than the Prado and Van Mier (2003) systems; however, the calculation effort turns out to be sizable, especially in determining the constitutive behavior parameters.

The second group of methods, i.e. using discrete elements, is based on modeling the continuum by means of rigid particles. The interaction laws between discrete elements serve to determine the macroscopic constitutive behavior. During early developments for non-cohesive materials like sands (Cundall and Strack, 1979), particle interactions were described by friction laws, but the interaction laws for cohesive materials have since become refined (Hentz *et al.*, 2004a).

Particle shapes remain of great importance. With a circular-shaped contact, determination is very fast even though porosity gets introduced. Polyhedrons (Issa and Nelson, 1992) fill the space very well, yet contact determination requires a specific and expensive algorithm that is more complex than for spheres or ellipsoids.

To guarantee reasonable computation times, a model based on Distinct Elements (Cundall and Strack, 1979) with rigid spheres has been chosen herein. Two types of

interactions are defined. The initial interactions between two elements are generally link interaction (the two elements are not necessarily in contact). Additional interactions of contact type can be added during the simulation. Interactions between two spheres are defined with normal K_n and tangential K_s stiffnesses characterizing the elastic behavior of concrete. "Micro-macro" relations (Eq. 1) from the Young's modulus and Poisson's ratio yield the local stiffnesses K_n and K_s. These relations stem from homogenization models (Liao *et al.*, 1997) typically used for regular DE assemblies; they have been modified to take into account both the relative disorder and the interaction surface S_{int}. Equation (1) shows the micro-macro relations applied to determining K_s and K_n between two elements *a* and *b*. $D_{init}^{a,b}$ stands for the initial distance between elements *a* and *b*, with R_a and R_b being the element radii. The α, β and γ parameters still need to be identified.

$$\begin{cases} E = \dfrac{D_{init}^{a,b}}{S_{int}} K_n \dfrac{\beta + \gamma \dfrac{K_s}{K_n}}{\alpha + \dfrac{K_s}{K_n}} \\[4mm] \nu = \dfrac{1 - \dfrac{K_s}{K_n}}{\alpha + \dfrac{K_s}{K_n}} \end{cases} \text{ or } \begin{cases} K_n = E \dfrac{S_{int}}{D_{init}^{a,b}} \dfrac{1 + \alpha}{\beta(1 + \nu) + \gamma(1 - \alpha\nu)} \\[4mm] K_s = K_n \dfrac{1 - \alpha\nu}{1 + \nu} \end{cases} \quad \text{Eq. (1)}$$

with: $S_{int} = \pi \left(\min(R_a, R_b)\right)^2$

Stiffnesses K_n and K_s are used to compute the normal and tangential forces, F_n and F_s. The sign convention employed herein is a positive compression force. An equivalent contact point P_c is used to calculate local tangential displacement and rotation. For an interaction between elements *a* and *b*, the distance between the centroid of element *a* and the equivalent contact point P_c is:

$$D = R_a + \frac{1}{2}(D^{a,b} - (R_a + R_b)) \cdot \qquad \text{Eq. (2)}$$

The aim of this study is to model very large structures or parts of structures. The interaction laws are therefore stated in order to best represent concrete behavior at the macroscopic scale. To model the nonlinear behavior of the material, a modified Mohr-Coulomb model with softening has been adopted (see Fig. 1). When the tangential force F_s lies outside the yield surface presented in the right-hand part of Figure 1, F_s is taken at its maximum value for the corresponding normal force F_n. Local parameters are the tensile strength T, cohesion C_o and softening factor ζ (both the friction Φ_i and contact Φ_c angles are not studied in this paper and have been assigned fixed values of 6°). These local parameters must be identified from global parameters, such as compressive and tensile strengths σ_c and σ_t. More sophisticated laws taking into account compaction phenomena can be elaborated but they are not necessary to model thin structures (like the slab we use in the last part) as flexion and tension effects are principally observed.
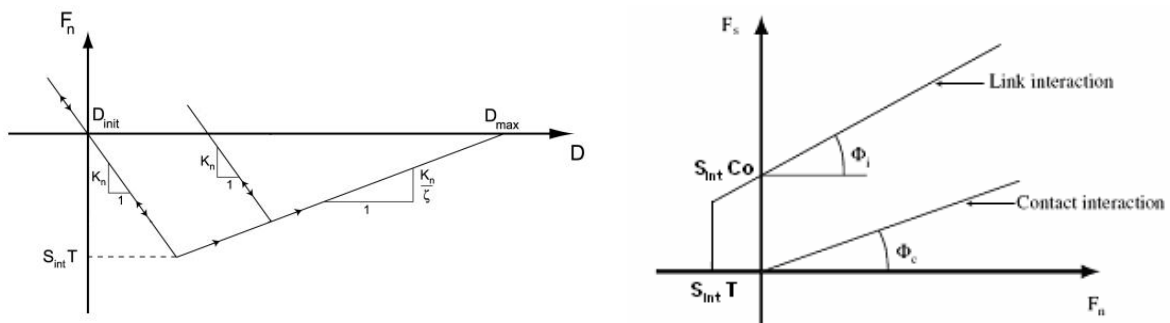
Fig. 1: Interaction laws for DE

Hentz *et al.* (2004a) established a procedure for identifying all material parameters based on a simulation of quasi-static compression and tension tests. These authors used an energy method to ensure that macroscopic parameters (Young's modulus) were not dependent on the various randomly-disordered DE samples.

The centroid positions are randomly generated through use of a special "disordering" technique (based on an algorithm described in Jodrey and Torry, 1985) that provides a polydisperse assembly with a particular size distribution. The characteristic sizes of elements

do have to be representative of concrete constituents, such as the granular or cement matrix, since the aim is to produce a macroscopic description. The number of discrete elements must therefore be as small as possible to maintain a reasonable computation time. The specimen however must contain enough elements to guarantee a minimum number of links along with a correct distribution.

Figure 2 shows the orientation distribution of the links present; this distribution is quasi-uniform for various DE samples, which ensures an isotropic macroscopic constitutive behavior for the concrete samples.
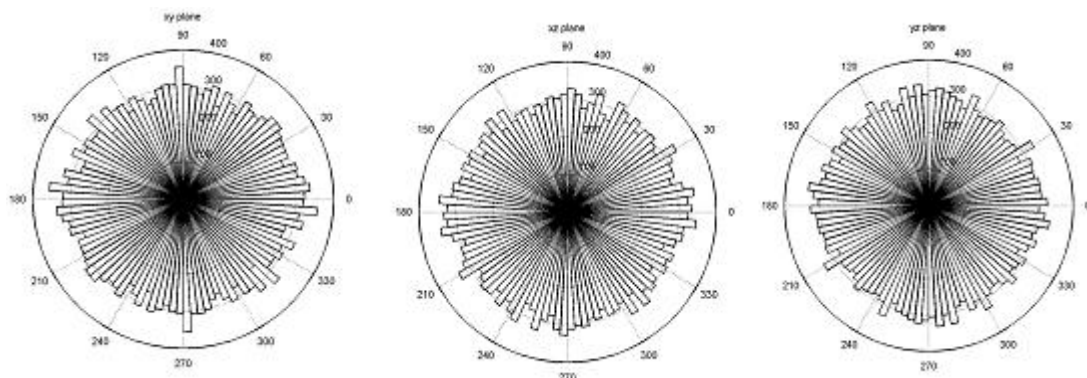
Fig. 2: Distribution of contact orientations within the sample

Initially, two discrete elements interact if the distance between their centroids is less than a given radius of interaction. According to the authors' experience, this radius of interaction is to be chosen such that the average number of interactions per DE equals 12: this value is the average number of links present in a regular (Face-Centered-Cubic) assembly of elements. Another value may be chosen, but such a change would introduce a different set of parameters. Of course this number cannot be too small to keep an isotropic specimen where there are not privileged directions of interactions.

As part of the proposed identification process and in order to obtain reliable results, this average number of interactions is calculated with internal elements only (i.e. edges are not considered). Young's modulus can thus be predicted with a maximum relative error of 6%.

It should be noted that in all of the following simulations, both axial and radial strains reflect the sample averages. For stability reasons, only those DE far from the edges and far from the central axis will be taken into account (Fig. 3).
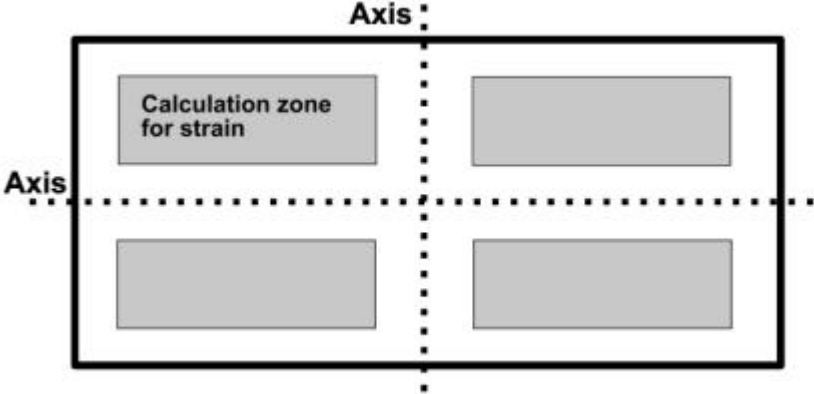

Fig. 3: DE taken into account when computing the average strain

2.2 Identification of linear parameters

Tests carried out using the α, β, γ values identified by Hentz *et al* (2004a) reveal an error of between 20% and 30% for Poisson's ratio and about 5% for Young's modulus. The α, β and γ values must be reestablished. First of all, for some values of K_s/K_n, the ratio E/E_0 and Poisson's ratio ν were computed (a $K_s/K_n=1$ yields the E_0 value), which produces the set of numerical points to be fitted. Figure 4 displays how Hentz's identification (dotted line) of α, β, γ does not fit the corresponding numerical points.
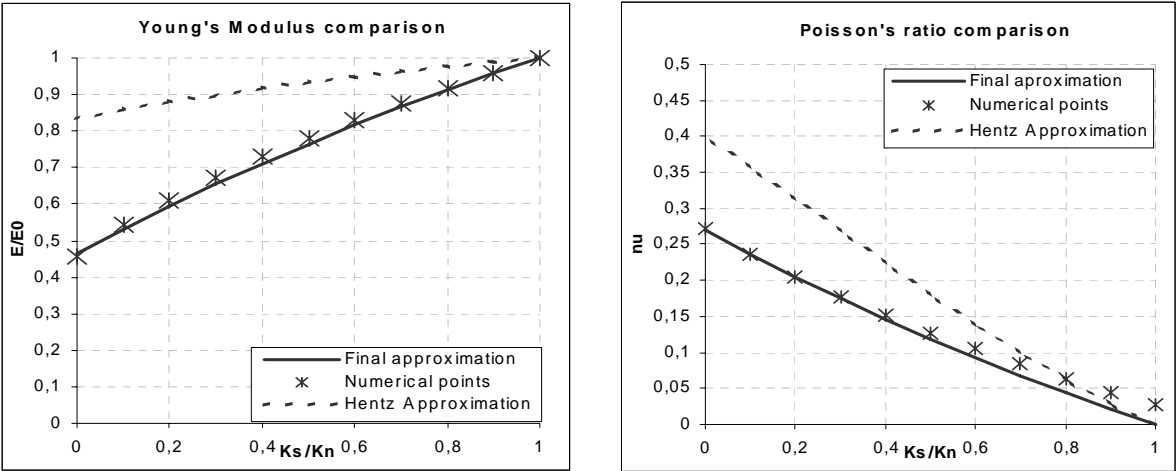
Fig. 4: Comparison of Young's modulus and Poisson's ratio computed and derived by approximation

The values of α, β, γ need to be changed. The best-fit approximation (solid line in Figure 4) is obtained with:

$$\begin{cases} \alpha = 3.7 \\ \beta = 2.198 \quad \text{with } \nu < 1/\alpha \ (0.27) \\ \gamma = 3.79 \end{cases} \qquad \text{Eq. (3)}$$

Hentz's values amount to:

$$\begin{cases} \alpha = 2.5 \\ \beta = 2.0 \quad \text{with } \nu < 1/\alpha \ (0.4) \\ \gamma = 2.65 \end{cases} \qquad \text{Eq. (4)}$$

Tests have been carried out on 16 samples, as presented in Table 1. The first 10 of these have identical sizes but different disorders, nos. 11 through 16 also display different geometries. The characteristic element size is identical for all samples, except no. 16. Sample nos. 15 and 16 have the same geometries, but no. 16 contains fewer elements with a larger average radius (1,427 DE vs. 18,672 DE).

Sample number	Length (m)	Width (m)	Height (m)
1 through 10	0.5	0.25	0.25
11	0.5	0.4	0.25
12	0.25	0.25	0.5
13	0.25	0.25	0.25
14	0.4	0.4	0.4
15 and 16	0.6	0.6	0.6

Table 1: Sample dimensions

With these new values of the α, β and γ parameters, the average uncertainty now stands at 2% (with a maximum error of 7%) for Young's modulus and at approx. 3% (maximum error of 6%) for Poisson's ratio: these results are highly accurate. The process employed to set the elastic behavior is now simpler in comparison to Hentz's proposal (2004). Hentz was required to conduct two uniaxial tensile or compressive tests, the first as a

reference for calculating the energy correction applied during the second. With this new identification of α, β and γ, the energy criterion proposed by Hentz is no longer needed. A correctly-adjusted interaction radius, which neglects border elements, guarantees accurate measurements of both the Young's modulus and Poisson's ratio during the first computation.

2.3 Identification of nonlinear parameters

The focus in this section is to identify local parameters for modeling macroscopic values, such as compressive strength σ_c and tensile strength σ_t.

As a first step, we have studied the reproducibility of both the compressive and tensile strength. A simulation of these uniaxial tests has been performed on the same set of samples as those used previously (Table 1). The parameters introduced here had been chosen arbitrarily and they are not held to be representative of any specific concrete.
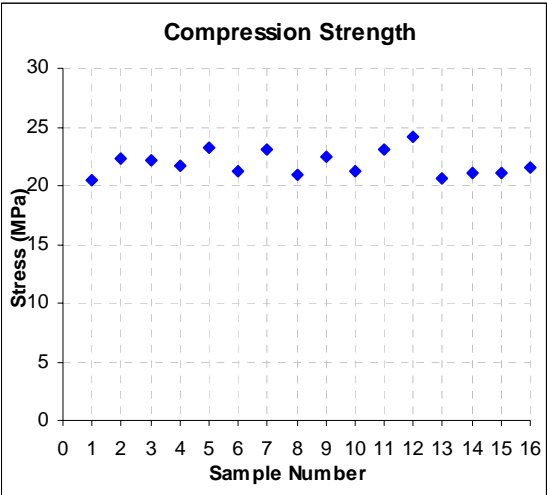
Fig. 5: Reproducibility of the compression limit   Fig. 6: Reproducibility of the tension limit
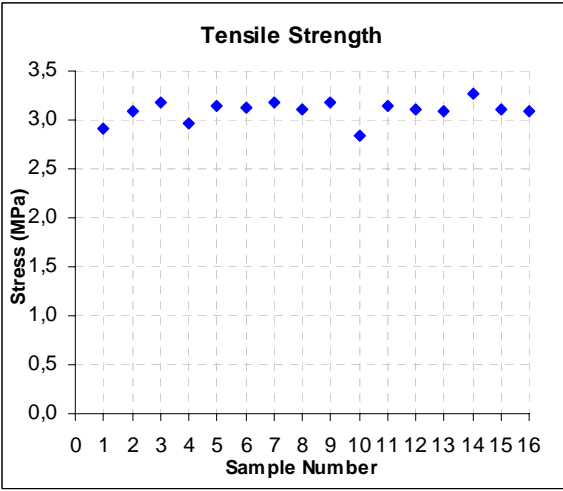
The level of reproducibility for both compressive strength (Fig. 5) and tensile strength (Fig. 6) is quite high. The gap between highest and lowest values equals about 2.6 MPa (6%) for compression and 0.3 MPa (5%) for tension.

These results suggest model reproducibility regardless of sample geometry or size and independently of the size of element used. From the perspective of modeling large structures, this identification process would be very expensive in terms of time, due to proportionality

with the number of elements. However, with reproducibility now demonstrated, a sample extracted from the entire large structure can yield the same results. The computation time required to determine behavioral parameters will therefore be reduced due to use of this extracted part. The sample must obviously be representative of the entire structure (i.e. not too small); in addition, it must be isotropic and attributed an adjusted interaction radius.

After exhibiting model reproducibility, we will now apply this identification process to determine actual concrete parameters. Identification work will be based on the R30A7 concrete studied at the 3S-R laboratory by Gabet *et al.* (2008).

This process will first involve uniaxial and quasi-static tensile tests to evaluate the local tensile strength T and softening parameter ζ. During a subsequent approach, compressive tests will lead us to the appropriate cohesion parameter C_o (Fig. 7).
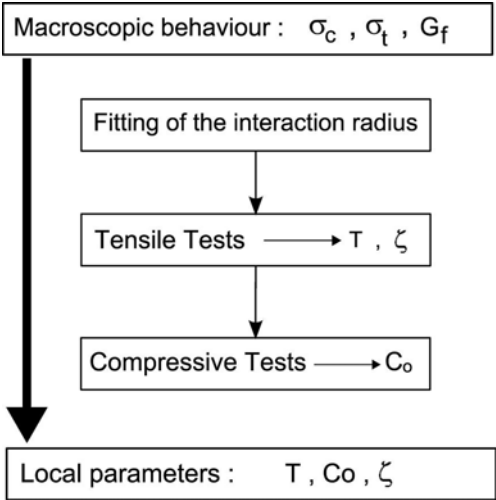
Fig. 7: The identification process

A local tensile strength T of 3.3 MPa and softening factor ζ of 10 provide for a rather good approximation of the experimental tensile test (Fig. 8). Even though the post-peak part of the experimental curve is not available, we can still observe a brittle behavior characteristic for the concrete material. The damage frame (Fig. 9) indicates a well-known tension crack. Damage is evaluated as the ratio of broken links to initial links and remains proportional to sphere darkness. The black color corresponds to free DE.
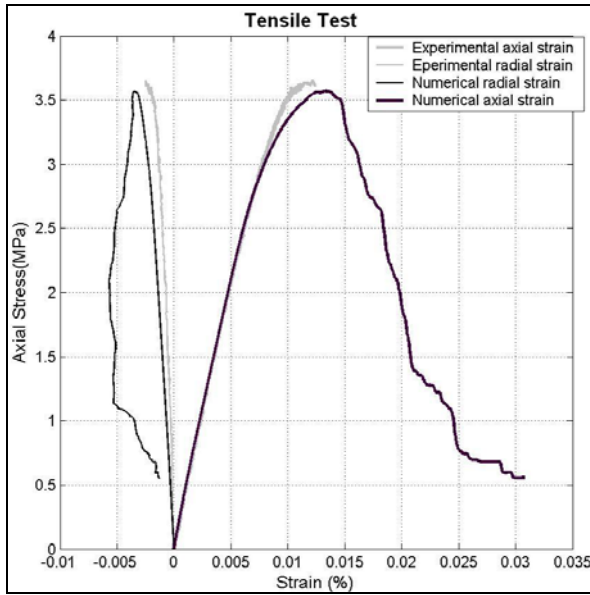
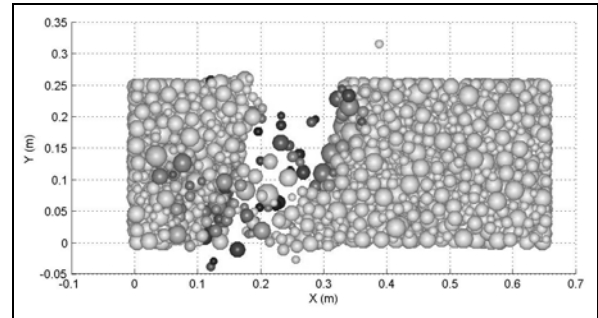| Fig. 8: Tensile test: Comparison of experimental and numerical results | Fig. 9: Damage in the sample at the end of the uniaxial tensile test |

The second test involves uniaxial and quasi-static compression. Results (see Fig. 10) appear to be suitable with Co = 4.4 MPa unless the last part of the experimental radial curve were to indicate otherwise. The damage shape reveals characteristic shear bands (Figs. 11 and 12).

With this identification process (Fig. 7), the Discrete Element Model can now accurately represent concrete behavior. As explained above, the identification time for a large structure would be reasonable when using a representative extracted part.
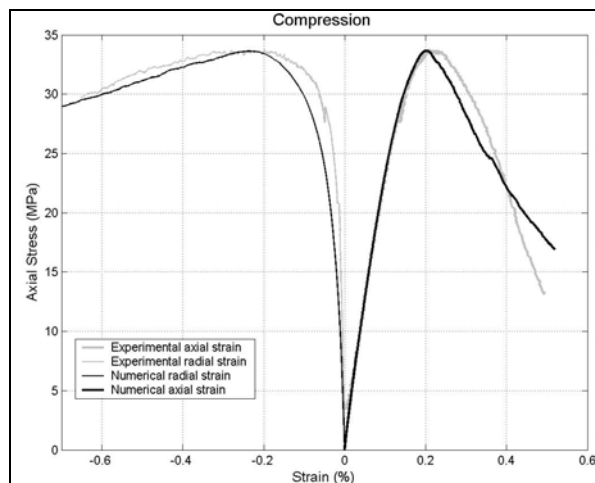
Fig. 10: Compressive test: Comparison of experimental and numerical results (complete graph and close-up)
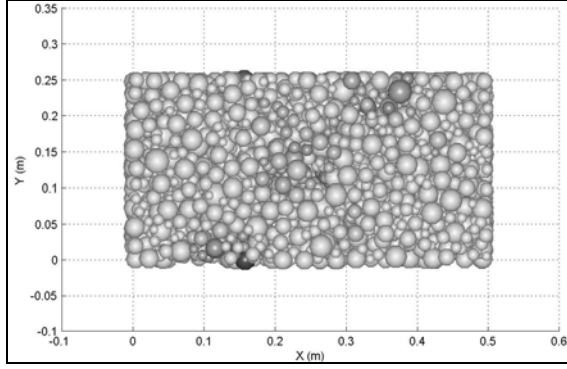
Fig. 11: Damage in the sample at peak stress of the uniaxial compressive test
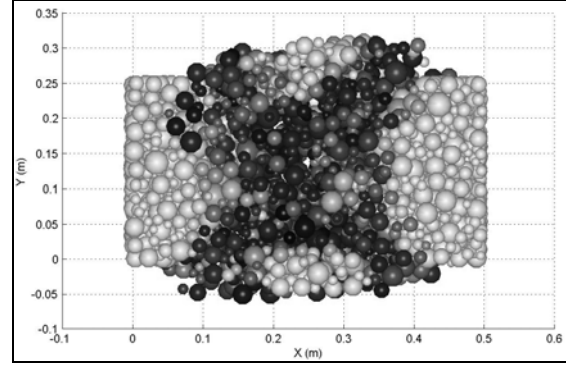

Fig. 12: Damage in the sample at the end of the uniaxial compressive test

3. Model description of the coupled method

Coupling methods have been widely studied. The first ones developed concerned the topic of Molecular Dynamics and Finite Elements at the microscopic scale. Curtin and Miller (2003) offered an overview of these atomistic methods; they introduced important notions, such as edge-to-edge coupling or bridging domain and energy weighting. Edge-to-edge methods typically require each Discrete Element to be coincident with a Finite Element node, which seems to be rather difficult within a disordered assembly. For this reason, edge-to-edge methods are naturally set aside. The bridging domain may be defined as a zone where MD and FE are both present and where the energy of both models is weighted. However, the bridging domain developed at the microscopic scale cannot be directly applied to a coupled DE-FE problem at the mesoscopic scale.

Xiao and Belytschko (2004) then developed a coupling method based on a bridging domain (Fig. 13) with energy weighting. Xiao's method proposes minimizing the Hamiltonian (H), which is the sum of the Hamiltonians of both the FE and DE.

$$H = \alpha H_{FE} + \beta H_{DE} \text{ with } H = E_{cin} + E_p \text{ and } \alpha + \beta = 1 \qquad \text{Eq. (5)}$$

where α and β are the weight parameter of the FE Hamiltonian and the DE Hamiltonian, respectively. α and β have been defined on Figure 13, which presents an example of the bridging domain with four FE layers.
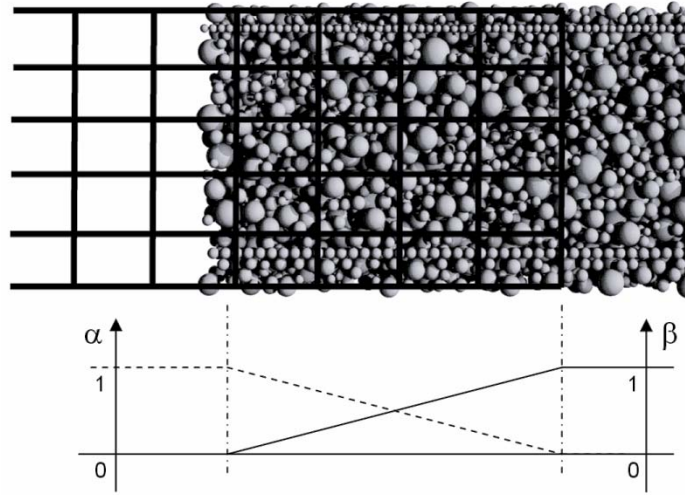
Fig. 13: Bridging domain and bridging parameter

To guarantee kinematic continuity, the degrees of freedom of both domains within the interface zone must be linked. Several approaches could be considered. Xiao and Belytschko (2004) proposed directly linking the Discrete Element degrees of freedom with Finite Element degrees of freedom using Lagrange multipliers. Eq. (6) presents the kinematic conditions on bridging domain r, with d DE displacements and u FE displacements.

$$\vec{d}_r = \bar{\bar{k}}.\vec{u}_r$$

Eq. (6)

The Arlequin method (BenDhia and Rateau, 2005) uses displacement and strain projections over shape functions, in assuming field continuity. This method enables a spatial relaxation of the kinematic conditions. With Discrete Element models, the displacement and strain are not known at all points and such projections are not simple to use. This method may be adapted to DE models, by approximating the displacement and deformation fields, although this would increase computation time.

The preferred method therefore calls for using rigid kinematic conditions, like those in Xiao and Belytschko (2004). Complementary kinematic constraints must then be added to link the DE rotations. Equation (7) lists the kinematic conditions linking DE rotations ω and displacements d with FE displacements u over bridging domain r. Both numerical simulations

and experimental results (Calvetti, 1997) have shown that DE rotations are equal to the antisymmetrical part of the displacement gradient.

$$\vec{d}_r = \bar{\bar{k}}.\vec{u}_r \text{ and } \vec{\omega}_r = \bar{\bar{h}}.\vec{u}_r \qquad \text{Eq. (7)}$$

We have derived the solution by minimizing Equation (8), with the kinematic conditions being taken in account using Lagrange multipliers λ^d for displacements and λ^ω for rotations.

$$H_g = H + \overrightarrow{\lambda^d}\left(\overrightarrow{d_r} - \bar{\bar{k}}\,\overrightarrow{u_r}\right) + \overrightarrow{\lambda^\omega}\left(\overrightarrow{\omega_r} - \bar{\bar{h}}\,\overrightarrow{u_r}\right) \qquad \text{Eq. (8)}$$

The time discretization relies upon an explicit scheme:

$$u(t + \Delta t) = 2u(t) - u(t - \Delta t) + \Delta t^2 \, \ddot{u}(t) \qquad \text{Eq. (9)}$$

Each degree of freedom value is calculated without taking in account coupling. Then a correction is applied using the Lagrange Multipliers (Eq. (8)). Further details on the method developed can be found in Frangin *et al.* (2006).

The difference in discretization size between FE and DE may induce wave reflection at the interface, an effect that can be mitigated in different ways, e.g. damping, yet the choice of damping coefficient is not straightforward. We have proposed a method to attenuate the reflection by introducing a reduction parameter for Lagrange multiplier influence. This method leads to a temporal relaxation of the kinematic constraints and is equivalent to a penalty method with an automatic process for optimizing the penalty parameter. All of these methods are discussed in Frangin *et al.* (2006). In the next section, the application presented introduces just such a relaxation parameter, which serves to divide the influence of Lagrange multipliers in reducing wave reflection.

4. A rock impact on a concrete slab

This section will present an application of both the coupling method and DE identification process. The full DE model will be compared with the coupling method, and the identification process explained above will be used in the two cases to determine local DE parameters.

This application consists of a rock impact on a concrete slab. A cubic rock block with a 30-cm side length impacts a concrete slab 2.5 m long, 2.0 m wide and 0.28 m thick. The velocity of the impacting object is set at 40 m/s. The two opposite sides are locked in the direction perpendicular to the medium slab plane. The slab is first divided into two parts: the center modeled by DE, and the sides modeled by FE with three bridging domain layers (Fig. 14). In a second model, only the DE are used.
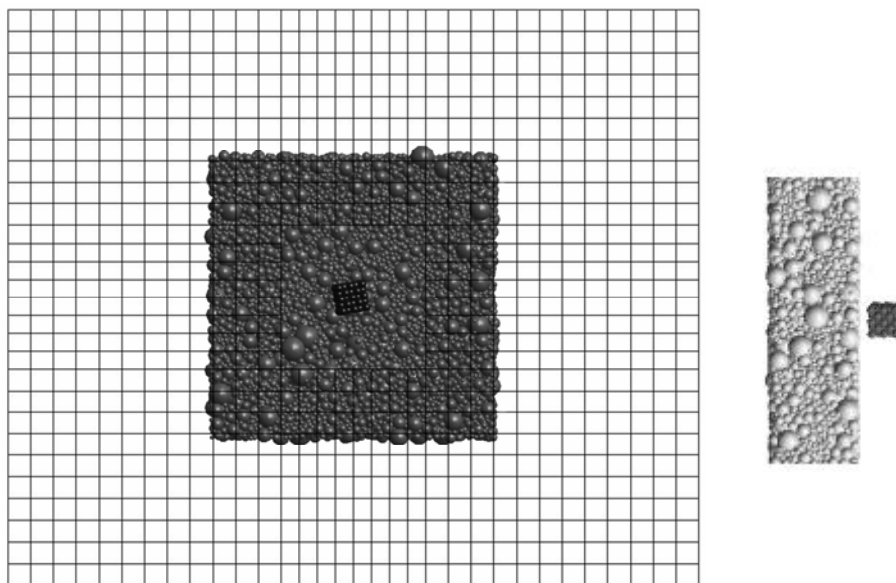
Fig. 14: Combined FE/DE model, and a side view of the DE part

In both models, the DE identification process previously described has been applied. A representative cube of the slab is extracted for identification purposes. This sample is isotropic, as shown by the orientation of interaction directions (Fig. 15). Moreover, the interaction radius is adjusted in order for the average number of interactions per element to equal 12. Sets of compression and tension computations are also performed to identify the

local concrete parameters. Such local parameters are determined so as to yield a tensile strength of around 3 MPa and a compressive strength in the vicinity of 20 MPa (Table 2).
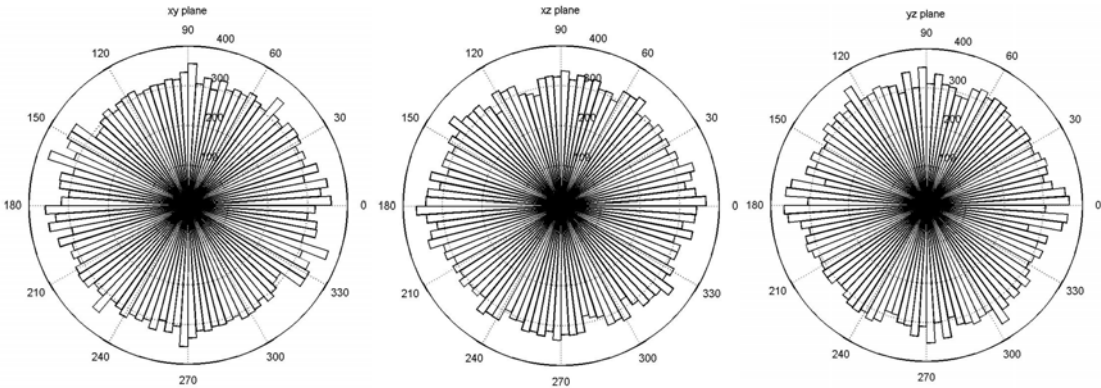

Fig. 15: Orientation of interaction directions for the extracted sample

T	C_0	ζ	Φ_i	Φ_c	E	ν
3.1 MPa	36 MPa	5	6°	6°	30 GPa	0.2

Table 2: Local concrete parameters

With these DE parameters, impact simulations are carried out using DE/FE in one model and DE only in the other. Figure 16 and 17 present comparisons of displacement between just the DE model (solid line) and the coupled DE/FE model (dashed line) at two different points. The maximum displacement predictions of both models are similar and, on the whole, the time response for the two models is the same.
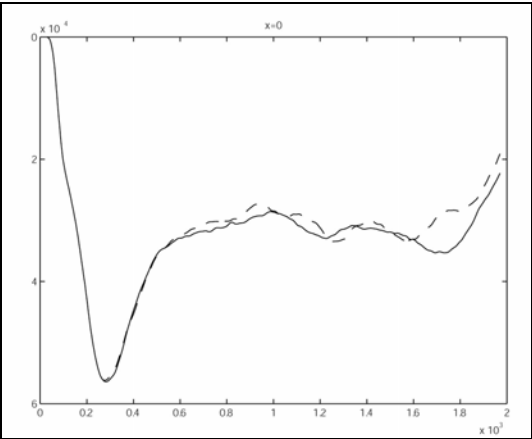
Fig. 16: DE displacement under the impacting object   Fig. 17: DE displacement vs. FE displacement
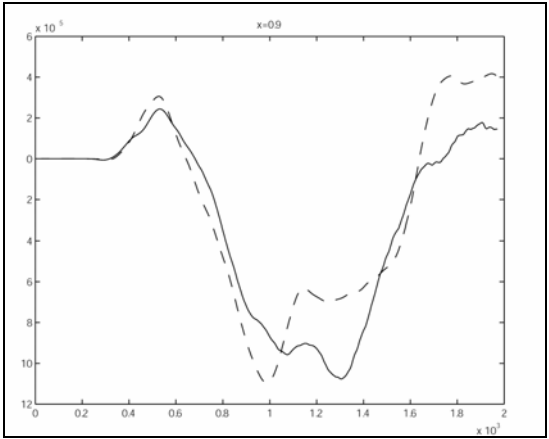
The combined model also efficiently describes damage in the vicinity of the impacted zone. In Figure 18, the damage obtained from the full DE approach and coupled DE/FE model

are compared simultaneously. Damage is measured as the ratio of broken links to initial links and remains proportional to sphere darkness. The black color corresponds to free DE.

The goal of this combined FE/DE model is to utilize the efficiency of DE to locally represent the fracture process on a large structure. A computation time analysis for this problem reveals that the coupled FE/DE model runs ten times faster than the full DE model (Table 3).

Model	DE	Coupled DE/FE
Number of DE	120808	6588
Number of FE node	0	5935
Number of time step	100000	100000
Duration of computation	42h50mn	3h39mn

Table 3: Comparison of the duration of the simulation

This difference in computation time stems from two points. The coupled model enables proceeding with a coarse discretization (FE discretization) on four-fifths of the structure. The time-savings offered by the smaller number of degrees of freedom can be increased by using a multi-time step algorithm, which makes the computation cost of this part negligible in comparison with the total computation cost.

Because of the DE contact check, the computation time in DE does not increase linearly with the number of DE. By reducing the simulation time, we are able to simulate larger or more complex structures and/or refine the discretization.
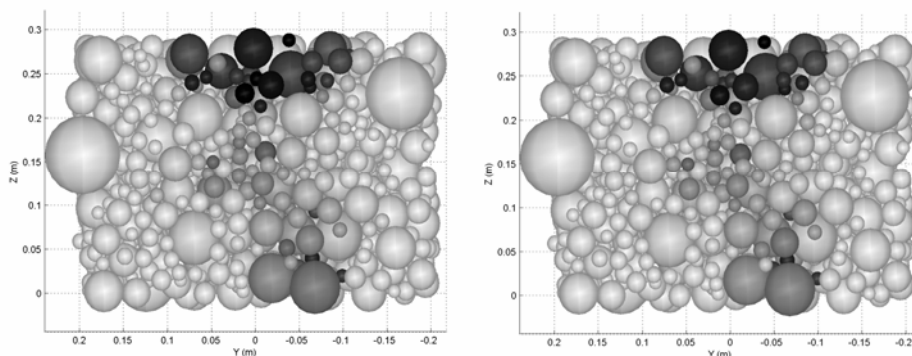

Fig. 18: Comparison of damage response between the full DE model (left) and coupled model (right)

5. Conclusion

The Discrete Element model offers an efficient and reliable means to represent concrete. A simple and effective process is now available and has been validated to identify local parameters. The reproducibility of results indicates that shape or size of the sample used to identify parameters exerts no influence. The identification for a large sample could thus be performed on a smaller sample extracted from the larger one. In addition, the computation time for model identification is reduced.

In contrast, the coupled approach seems to facilitate modeling a large structure submitted to local damage such as an impact. Comparative results between a full DE model and a combined model demonstrate that the two methods yield similar output, yet with a computation time ten times faster for the coupled method. We can therefore apply the coupled method to simulate an impact on very large structures, in recognition of the quality with which DE describes fractures and discontinuities.

References

Ben Dhia, H. (1998) "Problèmes mécaniques multi-échelles : La méthode Arlequin", *C. R. Acad. Sci. Paris*, **326**(Serie II b) 899-904.

Ben Dhia, H. and Rateau, G. (2005) "The Arlequin method as a flexible engineering design tool", *Int. J. Numer. Meth. Engng,* **62**,1442–1462

Berton, S. and Bolander, J. E. (2006) "Crack band model of fracture in irregular lattices", *Comput. Methods Appl. Mech. Engrg*., **192**, 7172-7181.

Calvetti, F., Combe, G. and Lanier, J. (1997) "Experimental Micromechanical Analysis of a 2D Granular Material: Relation Between Structure Evolution and Loading Path", *Mech. Cohesive-Frict. Mater.,* 2(2), 121-163.

Cusatis, G. and Cedolin, L. (2007) "Tow-scale study of concrete fracturing behavior", *Engng. Fract. Mech.*, **74**, 3-17.

Cundall, P. A. and Strack, O.D.L. (1979) "A discrete numerical model for granular assemblies", *Géotechnique*, **29**(1) 47-65.

Curtin, W.A. and Miller, R.E. (2003) "Atomistic/continuum coupling in computational material science", *Model. Simul. Mater. Sci. Eng.,* **11**(3) R33-R68.

Frangin, E. Marin, P. and Daudeville, L. (2006) "On the use of combined finite/discrete element method for impacted concrete structures", *J. Phys. IV France* **134,** 461–466.

Frangin, E. Marin, P. and Daudeville, L. (2006). "Discrete-continuum coupling for impacted structures", *Proceedings of the Eigth International Conference on Computational Structures Technology, B.H.V Topping, Civil-Comp Press, Stirling, United Kingdom, paper 167*.

Gabet, T. Malécot, Y. and Daudeville, L. (2008) "Triaxial behaviour of concrete under high stresses: Influence of the loading path on compaction and limit states", *Cem. Concr. Res.*, **38(3)**, 403-412.

Hentz S., Daudeville L. and Donze F. V. (2004a). "Identification and Validation of a Discrete Element Model for Concrete", *J. Eng. Mech.*, **130**, 709-719.

Hentz S., Daudeville L. and Donzé F. (2004b). "Discrete Element Modelling of Concrete Submitted To Dynamic Loading at High Strain Rate", *Comput. Struct.*, **82**, 2509-2524.

Issa, J.A. and Nelson, R.B. (1992) "Numerical analysis of micromechanical behavior of granular material", *Engng Computation*, **9**, 211-223.

Jodrey W., Torry E., (1985), "Computer simulation of close random packing of equal spheres", *Physical Review A*, **32**(4), 2347-2351

Kawai, T., (1978) "New discrete models and their application to seismic response analysis of structures", *Nucl. Engrg. Des.,* **48**, 207-229.

Leite, J.P.B., Slowik, V. and Mihasshi, H., (2004), "Computer simulation of fracture processes of concrete using mesolevel models of lattice structures", *Cem. Concr. Res.*, **34**, 1025-1033.

Liao, C.-L., Chang, T.-P., and Young, D.-H, (1997), ''Stress–strain relationship for granular materials based on the hypothesis of best fit.'' *Int. J. Solids Struct.*, **34**(31–32), 4087-4100.

Prado, E.P. and Van Mier, J.G.M. (2003) " Effect of particle structure on mode I fracture process in concrete", *Engng. Fract. Mech.*, **70**, 1793-1807.

Rousseau, J. Frangin, E. Marin, P. and Daudeville, L. (2007). "Some Aspects of DE/FE Combined Method: Model Identification and Combined Method", *Proceeding of COMPLAS 2007,* Barcelona, September.

Schlangen, E. and Garboczi, E. J. (1997) "Fracture simulations of concrete using lattice models: computational aspects", *Engng. Fract. Mech.*, **57**(2-3), 319-332.

Xiao, S.P. and Belytschko, T. (2004) "A bridging domain method for coupling continua with molecular dynamics", *Comput. Methods Appl. Mech. Engrg.* **193** 1645-1669.

List of figures

List of tables